

## In-Vitro Study on Organic-Inorganic Hybrid Composite of Graphene Oxide-Fe<sub>3</sub>O<sub>4</sub>/Doxorubicin/TiO<sub>2</sub> as a Targeted Drug-Delivery System

Samaneh Farjadfar<sup>1</sup>, Younes Kamari<sup>1</sup>, Payam Ghiaci<sup>2</sup>, Mehran Ghiaci<sup>1\*</sup>

<sup>1</sup>Department of Chemistry, Isfahan University of Technology, Isfahan, 8415683111, Iran.

<sup>2</sup>Department of Chemistry and Molecular Biology, University of Gothenburg, Gothenburg, Sweden.

**Corresponding Author:** Mehran Ghiaci, Department of Chemistry, Isfahan University of Technology, Isfahan, Iran, **Tel:** +98 3133913254; **Email:** mghiaci@cc.iut.ac.ir

**Received Date:** 15 Jun 2017

**Accepted Date:** 29 Aug 2017

**Published Date:** 04 Sep 2017

**Copyright** © 2017 Ghiaci M

**Citation:** Ghiaci M, Farjadfar S, Kamari Y and Ghiaci P. (2017). In-Vitro Study on Organic-Inorganic Hybrid Composite of Graphene Oxide-Fe<sub>3</sub>O<sub>4</sub>/Doxorubicin/TiO<sub>2</sub> as a Targeted Drug-Delivery System. *M J Dent.* 2(1): 017.

### ABSTRACT

In our present work, we report a novel targeted drug-delivery system by using a simple and cost-effective procedure. Firstly, magnetic graphene oxide (GO-Fe<sub>3</sub>O<sub>4</sub>) was prepared by chemical co-precipitation of Fe<sub>3</sub>O<sub>4</sub> magnetic nanoparticles on GO platelets and it was used as carrier for loading of doxorubicin (DOX), an anticancer drug. After loading DOX, in order to prevent the premature degradation of drug from GO-Fe<sub>3</sub>O<sub>4</sub>/DOX composite, it was coated with TiO<sub>2</sub>, an inorganic porous coating, by using titanium (IV) butoxide, as precursor. In this way the GO-Fe<sub>3</sub>O<sub>4</sub>/DOX/TiO<sub>2</sub> hybrid composite was synthesized. Then, the drug release of composites were monitored using UV-Vis absorbance technique and the results revealed that incorporation of porous TiO<sub>2</sub> coating, enhanced the drug entrapment and decreased the amount of drug release, in which at pH 7.4, 56% and 15% of DOX was released from uncoated and coated composites, respectively. Moreover, after studying the release rate at pH 5.4, corresponds to the endosomal pH of cancer cell, the results showed that drug release is pH-sensitive, because the release rate of DOX in the pH 5.4 noticeably enhanced, compared to pH 7.4. Also, the MTT assays of hybrid composite confirmed its superior responsive to cancer cell lines.

### KEYWORDS

Graphene Oxide; Doxorubicin; Porous Coating; Hybrid Composite; Targeted Drug-Delivery.

### INTRODUCTION

Nowadays cancer is one of the main cause of death in around the world so that, in each year it is responsible for more 13% of death incidence [1]. The World Health Organization in 2015 estimated that 84 million people were died by cancer in the last decade [2]. In addition, GLOBOCAN 2012 reported 14.1 million new cancer per year in the world and estimated that by 2025 this number will raise up to 19.3 million [3]. Currently, four conventional therapeutic strategies for cancer therapy are surgery, radiation, chemotherapy and immunotherapy. Among these, chemotherapy is more common used but it has many disadvantages like high toxicity and side effects of anti-cancer drugs on healthy cells [4, 5].

Doxorubicin (DOX) is one of the most commonly used and most effective therapeutic anticancer drugs that has a high

potency against of various cancers. In the other hand, DOX like the other anticancer drugs has severe side effects such as gastrointestinal disturbances, nausea, vomiting, hair loss, bone-marrow aplasia and congestive heart failure [6]. As regards to the importance of this matter, there is an urgent need to find the new strategies and materials for targeted drug delivery. In targeted drug delivery systems (TDDSs), suitable carriers can be utilized to protect anticancer drugs from premature degradation in body and also minimize their side effects on normal cells [7]. In this regard, so far a vast range of materials have been used as carrier in TDDSs for cancer therapy, such as polymeric nanoparticles and vesicles [3, 8], inorganic materials [9, 10], liposomes [11], micelles [12] and so on.

Among proposed carriers, graphene oxide (GO) have received increasing attention in TDDSs due to its intrinsic advantages such as high surface area for physical adsorption of drugs (through  $\pi$ - $\pi$  stacking), non-toxicity, high levels of cellular uptake, effective transportation capability and pH-dependent drug release behavior [13-16]. In addition, GO has numerous oxygen-containing functional groups like carboxyl groups, hydroxyl groups and epoxy which make it dispersible in physiological media [17]. These exclusive properties have made GO an ideal candidate for the targeted cellular delivery of anticancer drugs [18, 19].

Generally, a potent drug delivery system in cancer therapy must have the ability to deliver drugs to the target tissue while decreasing their side effects on normal tissues and also it must prevent premature degradation and perform a controlled release at the tumor site in response to a particular stimulus [7, 20]. For this purpose, to achieve the targeted delivery, GO could be functionalized with targeting ligands and in this way it could be quickly guided toward the tumor site [21]. Also, to prevent the premature release of drug before reaching to the target lesion, drug-loaded GO could be coated by a suitable coating.

In this study to deliver of doxorubicin, we used both of the targeting agent and appropriate coating in a drug delivery system, to targeted delivery and prevent the premature release of drug, respectively. In the first step, we modified GO with  $\text{Fe}_3\text{O}_4$  magnetic nanoparticles by chemical co-precipitation method and then DOX loaded on it through  $\pi$ - $\pi$  stacking interactions [22]. Hence, the GO- $\text{Fe}_3\text{O}_4$ /DOX magnetic composite was prepared for magnetic targeted delivery of the cancer chemotherapy drug. In the second step, to prevent the premature release of drug during the guidance of composite toward the target tissue we utilized a technique which has been introduced in our previous works. In these works we successfully used titanium dioxide as a porous inorganic coating, to decrease the release of various drugs in controlled drug delivery systems [23-25]. In continuous of our previous studies and expanding this technique, we used it along with a targeting aspect in a drug delivery system for cancer therapy. Therefore, GO- $\text{Fe}_3\text{O}_4$ /DOX composite was coated with  $\text{TiO}_2$  by titanium tetra n-butoxide, as precursor and in this way GO- $\text{Fe}_3\text{O}_4$ /DOX/ $\text{TiO}_2$  nanohybrid organic-inorganic composite was synthesized. Then, the in vitro drug release of synthesized nanohybrid composite was investigated by UV-Vis absorbance in simulated buffer solutions.

## EXPERIMENTAL

### Materials

Powder flake Graphite (purity > 99.9%), ferric chloride hexahydrate ( $\text{FeCl}_3 \cdot 6\text{H}_2\text{O}$ ), ferrous sulfate hepta-hydrate ( $\text{FeSO}_4 \cdot 7\text{H}_2\text{O}$ ),

$\text{NaNO}_3$ ,  $\text{H}_2\text{SO}_4$ ,  $\text{NH}_3$  and n-hexane were purchased from Merck. Doxorubicin (purity > 98%) was supplied from Exir pharmaceutical Co. of Iran. Titanium (IV) n-butoxide,  $\text{Ti}(\text{O-nBu})_4$  (97%), was obtained from Sigma-Aldrich. All of reagents and solvents were analytical grade and used without further purification. Human breast cancer cell line (MCF-7 cells) and human cervical cancer cell line (Hela cells) were supplied from pasture institute (Tehran, Iran).

### Characterization techniques

UV-Vis absorbance (UV-2100, UNICO Instrument Corp.) was utilized to quantify the content of drug in buffer solution. FTIR spectra were recorded by FTIR spectrophotometer (Jasco 680-plus) in the range of 400-4000  $\text{cm}^{-1}$ . To observe the morphology of coated and uncoated samples, a field emission scanning electron microscopy (FE-SEM) (HITACHI S-4160) in acceleration voltage of 15.0 kV was performed. Differential scanning calorimetry (DSC) of the samples were performed at 10  $^\circ\text{C}/\text{min}$  in the 30-400  $^\circ\text{C}$  temperature range (BÄHR-Thermoanalyse GmbH – DSC 302). The size distribution and zeta potential of the samples were detected by dynamic light scattering using a Zeta sizer (Ver 6.00, Malvern Instrument Ltd., UK) by diluting the samples to 0.1 mg/mL in deionized (DI) water at 25  $^\circ\text{C}$ . Surface area and pore size distribution of samples were measured by the BET equation and BJH method, respectively [26, 27]. Before the adsorption-desorption measurements, the sample was degassed in vacuum at 100  $^\circ\text{C}$  for 6 h.

### Synthesis of graphene oxide

Graphene oxide was synthesized by using an improved Hummers' method according to the following procedure: in the first step, 0.5 g graphene powder and 0.25 g  $\text{NaNO}_3$  were added to 12 mL sulfuric acid and vigorously stirred at 0 $^\circ\text{C}$  for 10 h and then 1.5 g  $\text{KMnO}_4$ , oxidative agent, was added dropwise to the reaction mixture. The reaction temperature was increased to 45  $^\circ\text{C}$  and stirred for another 1 h. In the second step, 25 mL DI water was added to the reaction mixture and heated to 98  $^\circ\text{C}$  for 30 min, followed by cooling down to 0  $^\circ\text{C}$  for 1 h. Finally, to complete the reaction, 100 mL DI water and 4 mL  $\text{H}_2\text{O}_2$  were added and reacted for 1 h. The obtained mixture was centrifuged and sequentially washed with 5% HCl solution (three times), and then washed several times with distilled water until the pH of the supernatant become neutral.

The obtained GO was sonicated for 30 min, filtered by filter paper and dried.

### Preparation of magnetic graphene oxide (GO- $\text{Fe}_3\text{O}_4$ )

In this section, through chemical co-precipitation of  $\text{Fe}_3\text{O}_4$  magnetic nanoparticles on GO platelets, the magnetic GO was prepared. For this purpose, 50 mg GO was dispersed in 100 mL

DI water under nitrogen atmosphere. Then, 64 mg  $\text{FeCl}_3 \cdot 6\text{H}_2\text{O}$  and excess amount of  $\text{FeSO}_4 \cdot 7\text{H}_2\text{O}$  were added to the mixture. Reaction temperature was increased to 70 °C and reacted for 1 h under nitrogen atmosphere. Finally, a solution of  $\text{NH}_3$  (2M) was added dropwise to the reaction mixture and stirred overnight. The  $\text{GO-Fe}_3\text{O}_4$  product was obtained by magnetic separation and washed with water and dried.

### Preparation of GO-Fe<sub>3</sub>O<sub>4</sub>/DOX composites

In this regard, initially 0.1 g  $\text{GO-Fe}_3\text{O}_4$  was added to 50 mL DI water and it was sonicated for 30 min to be dispersed completely. Then, different amounts of DOX (10, 20, 30 and 40 wt% relative to the  $\text{GO-Fe}_3\text{O}_4$ ) were added to the suspension and sonicated for another 30 min. After 24 h vigorous stirring, the obtained composites were dried using rotary evaporator at 70 °C. The information of prepared composites are summarized in Table 1.

**Table 1:** Feed composition and drug content of  $\text{GO-Fe}_3\text{O}_4/\text{DOX}$  composites.

Entry	Abbreviation	GO-Fe <sub>3</sub> O <sub>4</sub> (g)	DOX (g)
GO-Fe <sub>3</sub> O <sub>4</sub> /DOX (10%)	A1	0.1	0.01
GO-Fe <sub>3</sub> O <sub>4</sub> /DOX (20%)	A2	0.1	0.02
GO-Fe <sub>3</sub> O <sub>4</sub> /DOX (30%)	A3	0.1	0.03
GO-Fe <sub>3</sub> O <sub>4</sub> /DOX (40%)	A4	0.1	0.04

### Synthesis of GO-Fe<sub>3</sub>O<sub>4</sub>/DOX/TiO<sub>2</sub> hybrid composites

In this section, the  $\text{GO-Fe}_3\text{O}_4/\text{DOX}$  composites were coated with an inorganic coating to prevent the premature release of DOX (Scheme 1). In the first stage, 0.1 g of  $\text{GO-Fe}_3\text{O}_4/\text{DOX}$  (40%) (A4) composite was added to a round-bottom flask containing 50 mL dry n-hexane and stirred for 2 h at 25°C to be dispersed completely. In the next stage, to form a porous coating of  $\text{TiO}_2$  around the composite, different quantities of  $\text{Ti(O-nBu)}_4$  (30, 40, 50 and 60 wt% of  $\text{TiO}_2$  relative to composite) dissolved in 5 mL of n-hexane and was added dropwise to the mixture. To hydrolyse of  $\text{Ti(O-nBu)}_4$ , the required amount of DI water was added to the mixture and after 24 h, the reaction mixture was filtered and dried. The information of synthesized hybrid composites are summarized in Table 2.

**Table 2:** Different amounts of  $\text{TiO}_2$  coated on  $\text{GO-Fe}_3\text{O}_4/\text{DOX}$  composites.

Entry	Abbreviation	GO - Fe <sub>3</sub> O <sub>4</sub> / DOX (g)	TiO <sub>2</sub> (g)
GO-Fe <sub>3</sub> O <sub>4</sub> /DOX/TiO <sub>2</sub> (40%, 30%)	B1	0.1	0.03
GO-Fe <sub>3</sub> O <sub>4</sub> /DOX/TiO <sub>2</sub> (40%, 40%)	B2	0.1	0.04
GO-Fe <sub>3</sub> O <sub>4</sub> /DOX/TiO <sub>2</sub> (40%, 50%)	B3	0.1	0.05
GO-Fe <sub>3</sub> O <sub>4</sub> /DOX/TiO <sub>2</sub> (40%, 60%)	B4	0.1	0.06

### Drug release studies

In order to simulate the biological condition of body, the drug release of composites was investigated at the physiological temperature of 37 °C and pH 7.4. Moreover, for establishing environment similar to the cancer cells, we used a buffer solution with pH value of 5.4. These buffer solutions were prepared according to the same procedure in our previous works [23, 24]. The content of DOX in buffer solutions was quantified using UV-Vis absorbance at  $\lambda_{\text{max}} = 490 \text{ nm}$ .

### Kinetic and mechanism of drug release

In this section, to investigate the in vitro drug release behavior of the prepared hybrid composites, they were studied kinetically using various mathematical models such as zero order, first order, Higuchi, Weibull, Baker-Lonsdale and Korsmeyer-Peppas. The Baker-Lonsdale model has been described for microcapsules or microspheres according to the equation (1):

$$f_1 = \frac{3}{2} \left[ 1 - \left( 1 - \frac{M_t}{M_\infty} \right)^{\frac{2}{3}} \right] \frac{M_t}{M_\infty} = K_t \quad (1)$$

In this equation,  $M_t/M_\infty$  is a fraction of drug released at time  $t$  and  $k$  is the release rate constant which corresponds to the slope. To study the release kinetics, data obtained from in vitro drug release studies were plotted as  $[d(M_t/M_\infty)]/dt$  with respect to the root of time inverse [28].

### Cytotoxicity and cell viability assays

The in vitro cytotoxicity of  $\text{GO-Fe}_3\text{O}_4/\text{DOX}/\text{TiO}_2$  hybrid composite (B2) were investigated with MMT assay. For this purpose, MCF-7 and Hela cells were cultured in complete RPMI-1640 (Gibco, Scotland) medium supplemented with 10% fetal bovine serum and penicillin/streptomycin (100 units/ml). 200  $\mu\text{L}$  of cell suspension (at concentration of  $4 \times 10^4$  cells/well) was seeded into a 96-well U-bottom microplates (Nunc, Denmark) and incubated for 24 h at 37 °C in a humidified atmosphere of 5%  $\text{CO}_2$ . Then, serial dilutions of B2 (20  $\mu\text{L}$ ; final concentration: 0.5, 1, 2 and 4  $\mu\text{M}$ ) were added and incubated for another 48 h. In the last step, to evaluate the cell viability, 20  $\mu\text{L}$  of MTT solution (0.5% w/v) was added followed by incubation for 4 h. Then the media was replaced with 200  $\mu\text{L}$  of DMSO and the plate shaken for 20 min at 37 °C. Absorbance was quantified at 540 nm by an ELISA plate reader (Awareness, USA). Each experiment included six wells for each condition and results expressed as mean  $\pm$  standard deviation.

## RESULTS AND DISCUSSION

### FTIR spectroscopy analysis

(Figure 1) represents the FTIR spectra of the materials obtained at each step of the synthesis. The FTIR spectra of GO,  $\text{GO-Fe}_3\text{O}_4$  and  $\text{GO-Fe}_3\text{O}_4/\text{DOX}$  composites (A1-A4) are given in the Figure. 1a. In the spectrum of GO, the presence of the oxygen functionalities on GO was confirmed by different ab-

sorption bands. The broad and strong absorption bands found at 3400 and 1621  $\text{cm}^{-1}$  corresponds to the O–H stretching and bending vibrations, respectively. The appeared band at 1725  $\text{cm}^{-1}$  is assigned to the C = O stretching vibrations of the carboxylic acid groups. Also, the absorption bands at 1224 and 1054  $\text{cm}^{-1}$  are attributed to the vibration of C – O (epoxy) and C – O (alkoxy) groups [20, 29]. In the spectrum of GO-Fe<sub>3</sub>O<sub>4</sub>, the existence of a characteristic band at 584  $\text{cm}^{-1}$  is assigned to the Fe – O stretching vibrations [29, 30]. The spectrum of pure DOX shows prominent bands at 3433 (O – H), 2924 (C – H), 1723 (C = O), 1620 and 1581 (N – H), 1414 (C – C), 1282 (C – O – C) and 1087 (C – O)  $\text{cm}^{-1}$  [31, 32]. These bands are also appeared in the spectra of GO-Fe<sub>3</sub>O<sub>4</sub>/DOX composites (A1-A4) and slightly shifted to the lower wavenumbers. Moreover, it is observed that by increasing the DOX content from A1 to A4 (10-40%) the intensity of these bands is increased. These results confirm that DOX was successfully loaded onto GO-Fe<sub>3</sub>O<sub>4</sub>. The FTIR spectra of GO-Fe<sub>3</sub>O<sub>4</sub>/DOX /TiO<sub>2</sub> hybrid composites (B1-B4) are shown in (Figure 1b). For better comparison and understanding, the FTIR spectrum of amorphous TiO<sub>2</sub> also was added to the figure. According to the observed characteristic bonds for TiO<sub>2</sub>, the broad bands appearing at 450–600  $\text{cm}^{-1}$  in these spectra can be attributed to the vibration of the Ti–O–Ti bonds [23]. As can be seen, by increasing the TiO<sub>2</sub> amount from B1 to B4, the intensity of this broad band is increased.

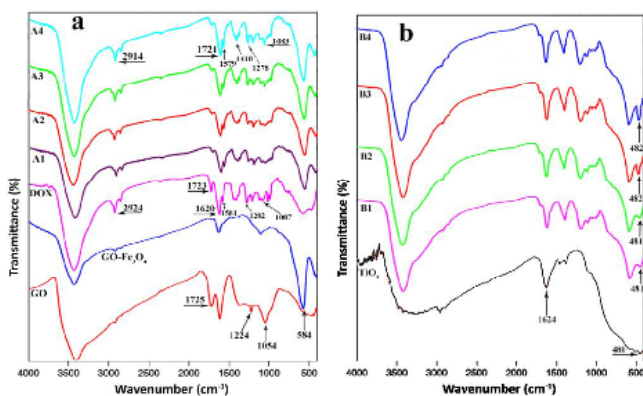


**Figure 1:** FT-IR spectra of (a) GO, GO-Fe<sub>3</sub>O<sub>4</sub>, DOX, A1, A2, A3, A4; (b) TiO<sub>2</sub>, B1, B2, B3, B4.

### Differential scanning calorimetry (DSC)

The DSC thermograms were plotted simultaneously to compare the thermal properties of DOX, GO-Fe<sub>3</sub>O<sub>4</sub>, GO-Fe<sub>3</sub>O<sub>4</sub>/DOX (40%) composite (A4) and GO-Fe<sub>3</sub>O<sub>4</sub>/DOX/TiO<sub>2</sub> (40%, 50%) hybrid composite (B3) in Figure. 2. For DSC of pure drug, DOX from the injection vial was first freeze-dried to obtain a dry powder. As can be seen, the thermogram of DOX exhibits a sharp endothermic peak at 218°C due to melting of the DOX ( $T_m = 218^\circ\text{C}$ ) [33]. In the case of GO-Fe<sub>3</sub>O<sub>4</sub> there is no peak in the range of used temperature, indicating that it has good thermal stability. In the thermogram of GO-Fe<sub>3</sub>O<sub>4</sub>/DOX (40%) composite (A4), the absence of a characteristic melting

peak of DOX between 150 and 260°C confirms that no pure drug was precipitated during composition and drug was uniformly dispersed in the texture of composite [34]. However, in the higher temperatures a low endothermic peak at 283 °C was appeared that it can be attributed to decomposition of A4 composite. In the thermogram of the GO-Fe<sub>3</sub>O<sub>4</sub>/DOX/TiO<sub>2</sub> (40%, 50%) hybrid composite (B3), a low endothermic peak at the higher temperature (332°C) was appeared that it shows the thermal stability of the composite was increased by coating with TiO<sub>2</sub>, compared to the uncoated composite [24]. These results could mean that the proposed method of gathering of the drug, matrix and inorganic coating has resulted to a uniform dispersion of the DOX in the GO-Fe<sub>3</sub>O<sub>4</sub> matrix with TiO<sub>2</sub> coating.

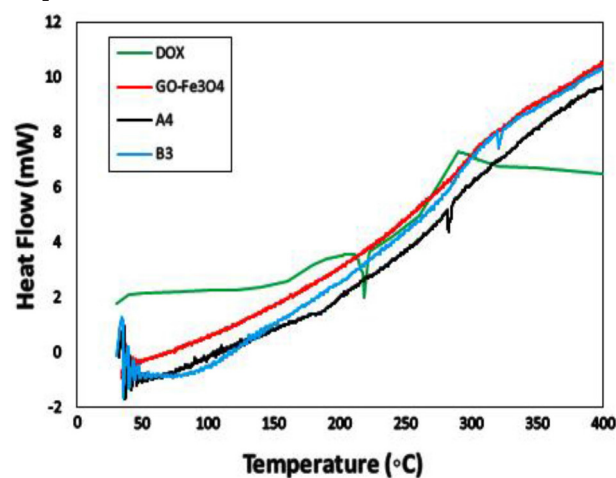


**Figure 2:** DSC thermograms of DOX, GO-Fe<sub>3</sub>O<sub>4</sub>, A4 and B3.

### Zeta potential and DLS measurements

To measure the stability of the samples in suspension state and to determine their size distribution, we used the zeta potential and DLS analysis, respectively and results given in Figure 3. For this purpose, zeta potential of the GO, GO-Fe<sub>3</sub>O<sub>4</sub>, A4 and B3 were measured by diluting the samples to 0.1 mg/mL in DI water without any additive at room temperature. As can be seen in the Figure. 3a, the zeta potential of GO illustrated a negative value (-45 mV) due to the abundance of OH and COOH groups. Compared to the GO, due to the positive charge of Fe<sub>3</sub>O<sub>4</sub> magnetic nanoparticles, the zeta potential of GO-Fe<sub>3</sub>O<sub>4</sub> increased slightly to -40 mV. In the case of A4 composite, the zeta potential again decreased to -51 mV due to existence of OH and COOH groups in the structure of DOX. Compared to A4, the zeta potential of B3 hybrid composite finally decreased to -58 mV due to abundance of OH groups on the surface of TiO<sub>2</sub>. Since a zeta potential of greater than  $\pm 30$  mV is considered sufficient for stabilisation of a colloidal suspension [35], so it can be concluded that prepared hybrid composite (B3) is stable in water. In the other words, B3 does not tend to coagulate in the water and so it can be utilized as

a good carrier in TDDSs. Moreover, for particle size determination of the samples, we applied the dynamic light scattering (DLS) analysis with experimental conditions similar to the zeta potential analysis and data given in the Fig. 3b. The z-average values for GO, GO-Fe<sub>3</sub>O<sub>4</sub>, A4 and B3 were obtained 92, 95, 115 and 126 nm, respectively.

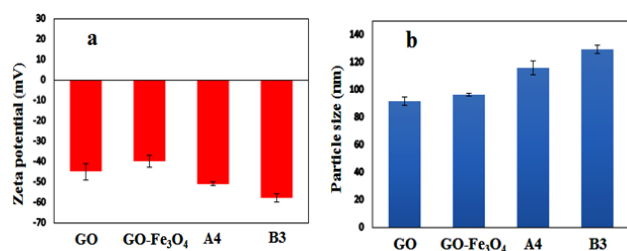


**Figure 3:** Zeta potential (a) and size distribution (b) of GO, GO-Fe<sub>3</sub>O<sub>4</sub>, A4 and B3.

### FE-SEM images

In order to observe the morphology of the optimum GO-Fe<sub>3</sub>O<sub>4</sub>/DOX composite (A4), before and after coating by amorphous TiO<sub>2</sub>, we used field-emission scanning electron microscopy (FE-SEM) analysis. The FE-SEM image of the GO-Fe<sub>3</sub>O<sub>4</sub>/DOX composite (A4) (Figure. 4a,b) revealed a sheet-like structure with different orientations and accumulated morphology [36]. According to the DSC thermogram of A4 composite we can judge that DOX is dispersed in the GO-Fe<sub>3</sub>O<sub>4</sub> matrix, so it can be concluded that the presence of a large number of oxygen-containing functional groups on the surface of GO and DOX, probably is the main factor of this accumulation [37]. After coating A4 composite with a porous TiO<sub>2</sub>, the morphology of the GO-Fe<sub>3</sub>O<sub>4</sub>/DOX/TiO<sub>2</sub> hybrid composite (B3) presented a uniform coating of porous TiO<sub>2</sub> on the surface of A4 composite (Figure 4c,d) [24,38]. It could be expected that by formation a porous shell of TiO<sub>2</sub> around A4 composite, the premature release of the DOX from GO-Fe<sub>3</sub>O<sub>4</sub> matrix would be reduced.

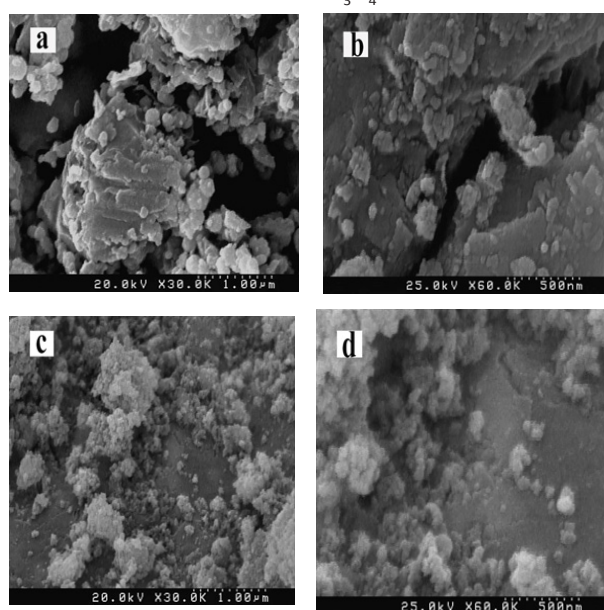


**Figure 4:** FESEM images of A4 (a,b) and B3 (c,d).

### N<sub>2</sub> adsorption–desorption isotherms

The representative N<sub>2</sub> adsorption–desorption isotherm and pore size distribution curve of GO-Fe<sub>3</sub>O<sub>4</sub>/DOX/TiO<sub>2</sub> (40%, 50%) hybrid composite (B3) are given in the Figure. 5a and 5b, respectively. Compared to the IUPAC definitions, it can be concluded that the B3 hybrid composite shows a type II adsorption–desorption isotherm [39]. Also, it has a specific surface area of 142.3 m<sup>2</sup>/g and exhibits a H3 hysteresis loop which it were reported for materials comprised of aggregate of plate-like particles forming slit shape pores [40]. As can be observed in the Figure. 5b, the pore size of B3 mainly distributed between 1.5-10 nm and the average of pore size was obtained 4.2 nm. Therefore, the prepared hybrid composite could be classified as a mesoporous solid [41].

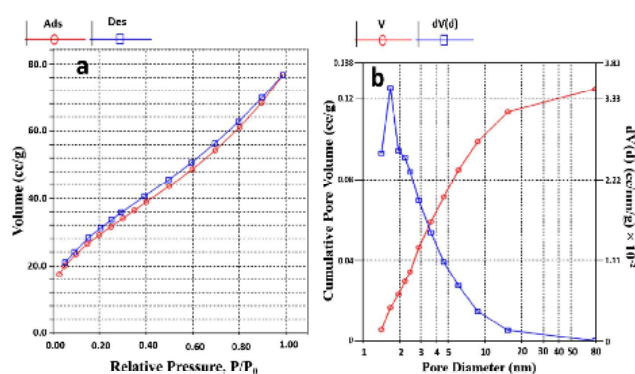
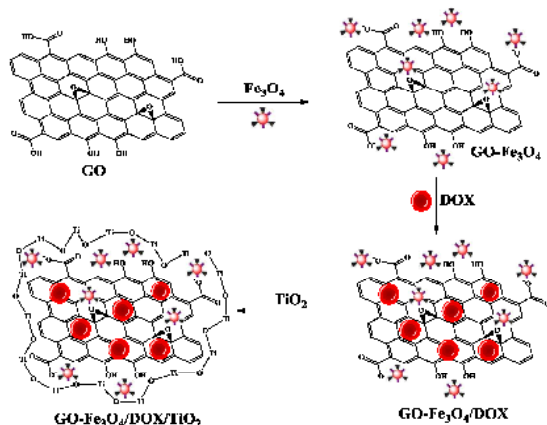


**Figure 5:** Nitrogen adsorption–desorption isotherms (a) and pore size distributions (b) of B3.

### Drug release studies

The DOX release tests were studied by suspending the prepared composites in simulated buffer solutions at 37 °C. For this purpose, the drug release profile was tested at pH 7.4 and 5.4, which correspond to the physiological pH and endosomal pH of cancer cell, respectively [42]. The release was monitored with UV-Vis spectrophotometry by observing the change in absorbance of the characteristics band of DOX at  $\lambda_{max} = 490$  nm. All experiments were done in triplicate and the results were averaged. In the first step, we examined the drug release of the GO-Fe<sub>3</sub>O<sub>4</sub>/DOX composites with 10, 20, 30 and 40 wt% of DOX (A1-A4) (Table 1). During the preparation of GO-Fe<sub>3</sub>O<sub>4</sub>/DOX composites, we expected that DOX adheres onto the surface of GO via strong  $\pi$ - $\pi$  stacking interactions. In addition, the NH<sub>2</sub> group of DOX is expected to form additional hydrogen bindings with OH groups of the GO. Figure. 6a represents the release profiles of DOX from the GO-Fe<sub>3</sub>O<sub>4</sub>/DOX composites in pH 7.4. As can be seen, there was an acceptable sustained release of the drug from all of the composites for 54 h, but dramatically they released about >30% of drug in the first 1 h and >40% after 3 h which it consider a negative point for a TDDS. Nevertheless, as we demonstrated in pre-

vious studies, this problem can be solved by formation of a porous inorganic coating like  $\text{TiO}_2$  around composites. Therefore in the second step, the composite containing 40 wt% of DOX (A4) (with highest correlation coefficient) was selected as optimum formulation and was coated by 50 wt% of  $\text{TiO}_2$  (Scheme 1).



**Scheme 1:** Schematic presentation of  $\text{GO-Fe}_3\text{O}_4/\text{DOX}/\text{TiO}_2$  hybrid composite formation mechanism.

In this way, according to the method mentioned in section 2.4, the  $\text{Fe}_3\text{O}_4/\text{DOX}/\text{TiO}_2$  (40%, 50%) hybrid composite (B3) was synthesized and drug release was examined once again. As can be observed in the Figure. 6b, the result was as expected and the coated composite (B3) released only 3% of DOX in the first 1 h and 6% after 2 h and also whole of drug was released after 120 h (data not shown). It is likely that  $\text{TiO}_2$  coating remains strongly on the composite through the strong hydrogen bonding interactions between composite and OH groups on the surface of  $\text{TiO}_2$ . Moreover, the formation of covalent bonds between the composite and  $\text{TiO}_2$  (during the hydrolysis of titanium tetra butoxide) could not be certainly rejected. In continuous, to investigate the effect of  $\text{TiO}_2$  amount on the drug release, the optimum composite (A4) was coated with different amount of  $\text{TiO}_2$ . Hence, other  $\text{GO-Fe}_3\text{O}_4/\text{DOX}/\text{TiO}_2$  hybrid composites with different amount of  $\text{TiO}_2$  were prepared (B1, B2 and B4) and their information summarized in Table 2. The drug release profiles of the B1, B2 and B4 composites were added to the Fig. 6b for better comparison. As is clear, for B1 and B2 with 30 and 40 wt% of  $\text{TiO}_2$  coating respectively, the amount of released DOX is increased compared to the B3 (with 50 wt%  $\text{TiO}_2$ ) while the performance of B4 (60 wt%  $\text{TiO}_2$ ) was about similar to B3. Based on the better performance (compared to B1 and B2) and lower amount of  $\text{TiO}_2$  (compared to B4), the  $\text{GO-Fe}_3\text{O}_4/\text{DOX}/\text{TiO}_2$  (40%, 50%) hybrid composite (B3) was selected as the optimum composite. In the last step, as the endosomal pH of cancer cells is slightly acidic, we used the buffer solution with pH of 5.4 to study the effect of pH on drug release. The results revealed that the release of DOX

from B3 is pH-dependent. As can be seen in the Figure. 6c, in slightly acidic solutions (pH 5.4) simulated to the reduced pH micro-environment typical of the cancerous cells, the release rate is significantly enhanced. In the pH 5.4, the amount of DOX released after 80 h is about 75% while in the pH 7.4 it was 15%. This difference may be caused by weakening of hydrogen bonds between the DOX and GO. Under acidic condition at pH 5.4, the  $\text{NH}_2$  group of DOX is protonated and  $\text{H}^+$  in solution would compete with the hydrogenbond-forming group and weaken the hydrogen bond interactions, as a result the DOX would faster release from composite.

Generally, the obtained results indicates that the  $\text{GO-Fe}_3\text{O}_4/\text{DOX}/\text{TiO}_2$  hybrid composite could be used as useful carrier in TDDS, because the pH-sensitive drug release could facilitate-hybrid composite to release its drug cargo in the acidic (pH < 6) endosomal environment after cellular uptake and increase the cytotoxicity toward cancer cells, while avoid injurious sideeffects in normal tissue.

The in vitro drug release data from various  $\text{GO-Fe}_3\text{O}_4/\text{DOX}/\text{TiO}_2$  hybrid composites (B1-B4) were investigated kinetically using various mathematical models. According to the obtained  $R^2$  values of the curves for various mathematical models, it was shown that there is a very good fitting between experimental data and Baker-Lonsdale model.

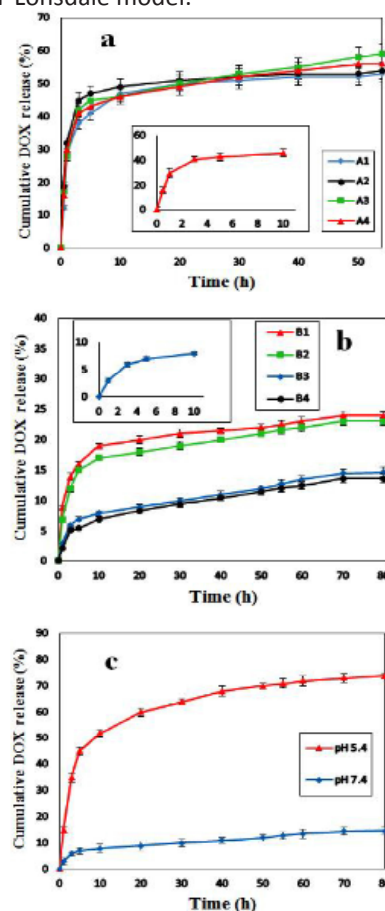


**Figure 6:** Cumulative DOX release (%) of A1-A4 at pH 7.4 (a); B1-B4 at pH 7.4 (b) and B3 in pHs of 7.4 and 5.4 (c).

### Cell viability assays

Figure 7a presents the viability of MCF-7 and Hela cancerous cells after treatment with different concentrations of GO-Fe<sub>3</sub>O<sub>4</sub>/DOX/TiO<sub>2</sub> hybrid composite (B3) after 48 h incubation time. When MCF-7 cells were treated with B3, they generally showed lower viability compared to Hela cells. As can be seen, different concentrations of B3 (0.5-4 μM) reduced viability of MCF-7 and Hela cells down to 41% and 26% respectively, which confirmed its superior responsive to cancer cell lines. Also, the cytotoxicity of GO-Fe<sub>3</sub>O<sub>4</sub>/TiO<sub>2</sub> composite (DOX free) against these cells with experimental conditions similar to the B3 was explored and results given in the Figure. 7b. As is clear, the DOX free composite shows very low cytotoxic effect on cancer cells which confirms its biocompatible and inert nature.

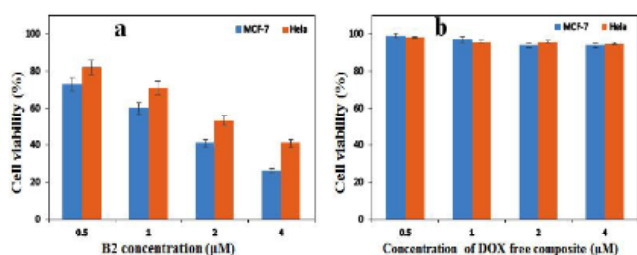


**Figure 7:** Cell viability of MCF-7 and Hela cells exposed to different concentrations of B3 (a) and GO-Fe<sub>3</sub>O<sub>4</sub>/TiO<sub>2</sub> (DOX free) (b) composites after 48 h incubation.

### ACKNOWLEDGMENTS

Thanks are due to the Research Council of Isfahan University of Technology and Center of Excellency in the Chemistry Department of Isfahan University of Technology for supporting of this work.

### REFERENCES

- Pramanika, Laha D, Dash SK, Chattopadhyay S, et al. (2016). An in-vivo study for targeted delivery of copper-organic complex to breast cancer using chitosan polymer nanoparticles. *Mater. Sci. Eng. C*. 68: 327-337.
- Travis WD, Brambilla E, Nicholson AG, Yatabe Y, et al. (2015). The 2015 World Health Organization classification of lung tumors: impact of genetic, clinical and radiologic advances since the 2004 classification. *Journal of Thoracic Oncology*. 10(9): 1243-1260.
- Masood F. (2016). Polymeric nanoparticles for targeted drug delivery system for cancer therapy. *Mater. Sci. Eng.* 60: 569-578.
- Cho K, Wang X, Nie S and Shin DM. (2008). Therapeutic nanoparticles for drug delivery in cancer. *Clin. cancer Res.* 14(5): 1310-1316.
- Soni G and Yadav KS. (2015). Applications of nanoparticles in treatment and diagnosis of leukemia. *Mater. Sci. Eng. C* 47: 156-164.
- Carvalho C, Santos RX, Cardoso S, Correia S, et al. (2009). Doxorubicin: the good, the bad and the ugly effect. *Curr. Med. Chem.* 16(25): 3267-3285.
- Moreira AF, Dias DR and Correia IJ. (2016). Stimuli-responsive mesoporous silica nanoparticles for cancer therapy: A review. *Microporous mesoporous Mater.* 236: 141-157.
- Liu Y, Gao FP, Zhang D, Fan YS, et al. (2014). Molecular structural transformation regulated dynamic disordering of supramolecular vesicles as pH-responsive drug release systems. *J. Control. Release* 173: 140-147.
- Huang WC, Hu SH, Liu KH, Chen SY, et al. (2009). A flexible drug delivery chip for the magnetically-controlled release of anti-epileptic drugs. *J. Control. Release* 139(3): 221-228.
- Puvvada N, Mandal D, Panigrahi PK and Pathak A. (2012). Aqueous route for the synthesis of magnetite nanoparticles under atmospheric air: functionalization of surface with fluorescence marker. *Toxicol. Res.* 1: 196-200.
- Torchilin V. (2008). Antibody-modified liposomes for cancer chemotherapy. *Expert Opin. Drug Deliv.* 5(9): 1003-1025.
- Markman JL, Rekechenetskiy A, Holler E and Ljubimova JY. (2013). Nanomedicine therapeutic approaches to overcome cancer drug resistance. *Adv. Drug deliv. Rev.* 5(13-14): 1866-1879.
- Sun X, Liu Z, Welsher K, Robinson JT, et al. (2008). Nanographene oxide for cellular imaging and drug delivery. *Nano Res.* 1(3): 203-212.
- Zhang D, Zhang Z, Liu Y, Chu M, et al. (2015). The short- and long-term effects of orally administered high-dose reduced graphene oxide nanosheets on mouse behaviors. *Biomaterials.* 68: 100-113.
- Long Y, Wang J, Tao C, Zhu H, et al. (2013). The loading and release properties of a novel drug carrier for benazepril based on nano graphene oxide. *J. Control. Release.* 1: e88-e89.
- Felber AE, Dufresne MH and Leroux JC. (2012). pH-sensitive vesicles, polymeric micelles, and nanospheres prepared with polycarboxylates. *Adv. Drug deliv. Rev.* 64(11): 979-992.
- Ma X, Tao H, Yang K, Feng L, et al. (2012). A functionalized graphene oxide-iron oxide nanocomposite for magnetically targeted drug delivery, photothermal therapy, and magnetic resonance imaging. *Nano Res.* 5(3): 199-212.
- Tao Ca, Wang J, Qin S, Lv Y, et al. (2012). Fabrication of pH-sensitive graphene oxide-drug supramolecular hydrogels as controlled release systems. *J. Mater. Chem.* 22(47): 24856-24861.
- Zhang L, Xia J, Zhao Q, Liu L, et al. (2010). Functional graphene oxide as a nanocarrier for controlled loading and targeted delivery of mixed anticancer drugs. *Small.* 6(4):

- 537-544.
20. Pan Q, Lv Y, Williams GR, Tao L, et al. (2016). Lactobionic acid and carboxymethyl chitosan functionalized graphene oxide nanocomposites as targeted anticancer drug delivery systems. *Carbohydr. Polym.* 151: 812-820.
  21. Lu J, Li Z, Zink JI and Tamanoi F. (2012). In vivo tumor suppression efficacy of mesoporous silica nanoparticles-based drug-delivery system: enhanced efficacy by folate modification, *Nanomedicine Nanotechnology. Biol. Med.* 8(2): 212-220.
  22. Jiang W, Yang HC, Yang SY, Horng HE, et al. (2004). Preparation and properties of superparamagnetic nanoparticles with narrow size distribution and biocompatible. *J. Magn. Magn. Mater.* 283(2-3): 210-214.
  23. Safari M, Ghiaci M, Jafari-Asl M and Ensafi AA. (2015). Nanohybrid organic-inorganic chitosan/dopamine/TiO<sub>2</sub> composites with controlled drug-delivery properties. *Appl. Surf. Sci.* 342: 26-33.
  24. Kamari Y and Ghiaci M. (2016). Preparation and characterization of ibuprofen/modified chitosan/TiO<sub>2</sub> hybrid composite as a controlled drug-delivery system. *Microporous mesoporous Mater.* 234: 361-369.
  25. Safari M, Kamari Y, Ghiaci M, Sadeghi-aliabadi H, et al. (2016). Synthesis and characterization of insulin/zirconium phosphate@TiO<sub>2</sub> hybrid composites for enhanced oral insulin delivery applications. *Drug Dev. Ind. Pharm.* 43(5): 1-9.
  26. Brunauer S, Emmett PH and Teller E. (1938). Adsorption of gases in multimolecular layers. *J. Am. Chem. Soc.* 60(2): 309-319.
  27. Barrett EP, Joyner LG and Halenda PP. (1951). The determination of pore volume and area distributions in porous substances. I. Computations from nitrogen isotherms. *J. Am. Chem. Soc.* 73(1): 373-380.
  28. Dash S, Murthy PN, Nath L and Chowdhury P. (2010). Kinetic modeling on drug release from controlled drug delivery systems. *Acta Pol Pharm* 67(3): 217-223.
  29. Zhao D, Gao X, Wu C, Xie R, et al. (2016). Facile preparation of amino functionalized graphene oxide decorated with Fe<sub>3</sub>O<sub>4</sub> nanoparticles for the adsorption of Cr (VI). *Appl. Surf. Sci.* 384: 1-9.
  30. Rani GJ, Babu KJ and Rajan MJ. (2016). Watsonia meriana flower like Fe<sub>3</sub>O<sub>4</sub>/reduced graphene oxide nanocomposite for the highly sensitive and selective electrochemical sensing of dopamine. *J. Alloys Compd.* 688: 500-512.
  31. Unsoy G, Khodadust R, Yalcin S, Mutlu P, et al. (2014). Synthesis of Doxorubicin loaded magnetic chitosan nanoparticles for pH responsive targeted drug delivery. *Eur. J. Pharm. Sci.* 62: 243-250.
  32. Balan V, Dodi G, Tudorachi N, Ponta O, et al. (2015). Doxorubicin-loaded magnetic nanocapsules based on N-palmitoyl chitosan and magnetite: Synthesis and characterization. *Chem. Eng. J.* 279: 188-197.
  33. Oliveira MS, Mussi SV, Gomes DA, Yoshida MI, et al. (2016). Ferreira, α-Tocopherol succinate improves encapsulation and anticancer activity of doxorubicin loaded in solid lipid nanoparticles. *Colloids Surfaces B Biointerfaces.* 140: 246-253.
  34. Manocha B and Margaritis A. (2010). Controlled release of doxorubicin from doxorubicin/γ-polyglutamic acid ionic complex. *J. Nanomater.* 12.
  35. Greenwood R. (2003). Review of the measurement of zeta potentials in concentrated aqueous suspensions using electroacoustics. *Adv. Colloid Interface Sci.* 106: 55-81.
  36. Atchudan R, Edison TNJI, Perumal S, Karthikeyan D, et al. (2017). Effective photocatalytic degradation of anthropogenic dyes using graphene oxide grafting titanium dioxide nanoparticles under UV-light irradiation. *J. Photochem. Photobiol. A Chem.* 333: 92-104.
  37. Masoudipour E, Kashanian S and Maleki N. (2017). A Targeted Drug Delivery System Based on Dopamine Functionalized Nano Graphene Oxide. *Chem. Phys. Lett.* 668: 56-63.
  38. Kamari Y and Ghiaci M. (2016). Incorporation of TiO<sub>2</sub> coating on a palladium heterogeneous nanocatalyst. A new method to improve reusability of a catalyst. *Catal. Commun.* 84: 16-20.
  39. Leofanti G, Padovan M, Tozzola G and Venturelli B. (1998). Surface area and pore texture of catalysts. *Catal. Today* 41: 207-219.
  40. Kruk M and Jaroniec M. (2001). Gas adsorption characterization of ordered organic-inorganic nanocomposite materials. *Chem. Mater.* 13(10): 3169-3183.
  41. Albarran L, López T, Quintana P and Chagoya V. (2011). Controlled release of IFC-305 encapsulated in silica nanoparticles for liver cancer synthesized by sol-gel. *Colloids Surfaces A Physicochem. Eng. Asp.* 384(1-3): 131-136.
  42. Gerweck LE and Seetharaman K. (1996). Cellular pH gradient in tumor versus normal tissue: potential exploitation for the treatment of cancer. *Cancer Res.* 56(6): 1194-1198.